Thermodynamic Basis of Isothermal Carbothermic Reduction of Oxide in Liquid Steel for Simultaneous Analysis of Soluble/Insoluble Oxygen Contents in the Steel Specimens

YOUN-BAE KANG, YONG-MIN CHO, and HAE-MI HONG

Oxygen in liquid steel exists as soluble O (chemically dissolved in the steel matrix) and insoluble O (physically dispersed as the oxide inclusion). To measure the soluble O content ([S.O]) and the insoluble O content ([I.O]), both in the context of gas fusion analysis technique such as inert gas fusion infrared absorption method, it is necessary to melt the specimen under a C saturation condition in a "two-stage" isothermal heating mode. The first stage is carried out at a low temperature (T_L), where only soluble O is extracted as CO(g). The second stage is subsequently carried out at a high temperature (T_H), where the oxide inclusion is reduced by a carbothermic reaction. Therefore, it is necessary to identify the carbothermic reduction temperature of the oxide inclusion in the liquid steel at the C saturation ($T_{M_xO_y}^{Fe}$). A series of CALPHAD-type thermodynamic calculations were carried out to estimate the temperature of each oxide inclusion (Al_2O_3, Fe_tO, SiO_2, CaO, and MgO). It was found that the temperature depends on the metal content ([pct M]) and total pressure (P) inside the gas fusion chamber: increasing [pct M] or P increases $T_{M_xO_y}^{Fe}$. The proposed method may be applied for the steel systems containing those inclusions except for Fe_tO. In the case of Al_2O_3 inclusion containing steel ([pct Al] = 0.04), for example, $T_{Al_2O_3}^{Fe}$, lies in the range of 1791 K (1518 °C) to 1838 K (1565 °C) depending on P inside the gas fusion chamber. Possible range of the $T_{M_xO_y}^{Fe}$ is reported.

I. INTRODUCTION

IDENTIFYING existence and distribution of non-metallic inclusions in steel is one of the most important things to deal with by steelmakers to control cleanliness of the steel product.[1,2] Recently, its cleanliness has been more emphasized during a tundish process, since the process is the final stage for the steel cleanliness control in steel production.[3] Evolution of the inclusions in the steel and understanding them are therefore an interesting topic in high-temperature steel processing.[4,5] In this regard, accurate, fast, and reliable analysis of the steel cleanliness is required. Apart from routine use of electron microscopy, the recent advance of a developing cathodoluminescence technique provides a rapid and prommissing tool to detect various types of oxide inclusions in steel specimens.[6] In addition to this, an accurate, fast, and reliable analysis of O content in steel specimens is very important to assess the cleanliness of the steel.

The most popular method of O content analysis is the inert gas fusion infrared absorption method. It has been used to provide total oxygen content ([T.O]) in the steel specimen. The principle of the analysis is (1) carbothermic heating of a steel specimen in a graphite crucible in a gas fusion chamber, (2) generating CO (and CO_2)*

*Hereafter, only CO(g) is mentioned.

---

gas, which is carried by He carrier gas, (3) measuring the extent of absorption of infrared ray's intensity by NDIR (Non-Dispersive InfraRed) sensor, (4) converting the extent to the amount of O in the specimen, and (5) reporting the "total" O content in the specimen.[7] The heating is carried out at a temperature high enough to extract nearly all the O in the specimen, whatever its form.

YOUN-BAE KANG, YONG-MIN CHO, and HAE-MI HONG are with the Graduate Institute of Ferrous and Energy Materials Technology, Pohang University of Science and Technology, Pohang, Kyungbuk 37673, Republic of Korea. Contact e-mail: ybkang@postech.ac.kr

Usually, the steel specimen contains O dissolved in the steel matrix (soluble O) and O in the form of oxide inclusion. Therefore, the "total O content" ([T.O]) is indeed a sum of "soluble O content" ([S.O]) and "insoluble O content" ([I.O]). In this conventional "one-stage" gas fusion analysis, all the oxygens are carburized to generate the CO(g) by heating the specimen at very high temperature, regardless of their original form. The oxide inclusion is reduced by the following carbothermic reduction:

$$M_xO_y(s) + y\underline{C} = yCO(g) + x\underline{M}; \\ \Delta G^\circ_{(1)} = \Delta H^\circ_{(1)} - T \times \Delta S^\circ_{(1)} \qquad [1]$$
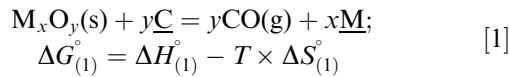
where M is a deoxidizing element such as Al, Si, *etc*. $\Delta H^\circ_{(1)}$ for this type of reduction is generally positive. The soluble O in the steel matrix also reacts with C to form CO(g)

$$\underline{O} + \underline{C} = CO(g); \ \Delta G^\circ_{(2)} = \Delta H^\circ_{(2)} - T \times \Delta S^\circ_{(2)} \qquad [2]$$
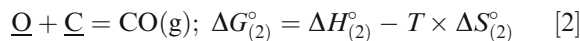
where $\underline{O}$ and $\underline{C}$ are the soluble O and the C already in the liquid steel or dissolved from the graphite crucible. Therefore, the "one-stage" gas fusion analysis only provides [T.O].

Recently, the present authors have proposed a simple but promising method for simultaneous analysis of [S.O] and [I.O] in steel specimens.[8] It uses a commercially available gas fusion analysis technique such as the inert gas fusion infrared absorption method. In the "two-stage" gas fusion analysis, the chamber was first heated to relatively lower temperature (T_L) where only Reaction [2] proceeds. This generates CO(g), which was formed from the soluble O. To facilitate Reaction [2], the T_L should be higher than the melting temperature of the steel specimen saturated by C. Then, the chamber was subsequently heated to a higher temperature (T_H) where Reaction [1] proceeds. This generates second CO(g), which was formed from the insoluble O (oxide inclusion). The T_H should be higher than the carbothermic reaction temperature of the oxide $T^{Fe}_{M_xO_y}$. By doing this, two different types of O can be separated in a single run of the gas fusion analysis. Therefore, it does not require any new equipment. The method can be used with already available inert gas fusion infrared absorption equipment only by changing the heating pattern. The core idea is shown in Figure 1.[8]

By this method, it is possible to identify the actual form of O (either dissolved in the steel matrix or suspended as an oxide inclusion) in a short time within a few minutes. One of the recent studies by the present authors on the reoxidation of ultra-low C (ULC) steel by Fe$_t$O-containing slag showed a rapid increase [T.O] due to the slag even at very low Al content.[9] The analyzed [T.O] was most likely [S.O], but the conventional "one-stage" gas fusion analysis could not clearly identify the actual form of the O. No such attempt to distinguish the two different types of O in steel was reported within the framework of gas fusion analysis. Alternatively, [I.O] could be measured by a slime method in which a steel specimen is dissolved in a solution with or without an electrolytic cell. This method is usually applied to observe non-metallic inclusions in the steel (size and shape), which are collected on a filter after the dissolution. Analyzing their mass eventually yields [I.O] content, assuming that the chemical formulae of the inclusions and their relative fractions are known.[10–13] However, it is laborious work requiring long extraction times and a large mass of the steel.[14] A solid-oxide type galvanic sensor can be also be used to measure [S.O] in liquid steel,[15,16] assuming that [S.O] is equivalent to the activity of O in the liquid steel. However, this method is also limited because of the long time for the measurement. Moreover, choice of the solid-oxide electrolyte might influence the measured EMF results.[16,17] With this in mind, the proposed "two-stage" gas fusion analysis is seen to be attractive thanks to its short analysis time (a few minutes compared to more than hours in the other methods).[8] This method was also applied to other Al-killed steels of various C contents.[18] It was reported that cleanliness of the steel may be influenced by supersaturation phenomena.[19–21] Analysis of the supersaturation phenomena requires [S.O].

In the present article, the thermodynamic basis of the proposed "two-stage" gas fusion analysis is discussed using available thermodynamic data. A possibility of Reaction [2] before the carbothermic reaction (Reaction [1]) is examined. This is the core idea of the proposed "two-stage" gas fusion analysis.

II. THERMODYNAMIC CONSIDERATION OF CARBOTHERMIC REDUCTION OF VARIOUS OXIDES

Suppose that a system contains the following elements: Fe, M, C, and O ($c = 4$), where the M is the metal element for deoxidation such as Al or Si. Also the system is composed of some of the following phases: liquid steel, graphite, oxide inclusion, and gas. The steel is contained in a graphite crucible; therefore, the graphite is always stable. At a low temperature ($T < T^{Fe}_{M_xO_y}$), the gas phase may not evolve. On the other hand, at a high temperature ($T > T^{Fe}_{M_xO_y}$), the oxide inclusion may disappear as a result of the carbothermic reaction, leaving the gas phase. At the condition of the carbothermic reduction, there are four phases ($p = 4$). At a constant pressure inside the gas fusion reaction chamber (P), the degree of freedom f of this system is $c - p + 2(-1) = 4 - 4 + 1 = 1$. Therefore, only one thermodynamic variable is to be set to find the $T^{Fe}_{M_xO_y}$. It may be a chemical potential of M or O in the liquid steel (proportional to the component's content), except for that of C**. Since the carbothermic reaction

---

**This is because the system is already in C-saturation condition ($a_{C(s)} = 1$).

(Reaction [1]) does not involve O explicitly, the metal content [pct M] should be the controlling
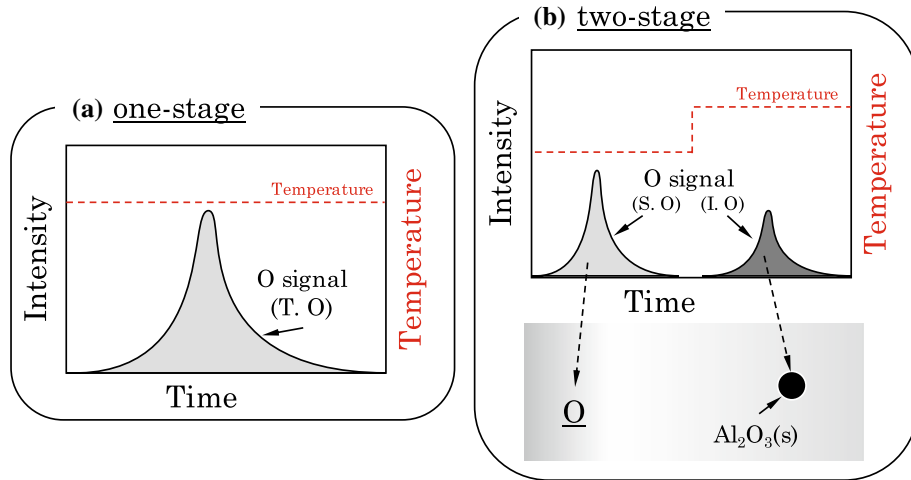
Fig. 1—A schematic representation of the conventional "one-stage" gas fusion analysis and "two-stage" gas fusion analysis[8] Reprinted with permission from Iron and Steel Institute of Japan (ISIJ), under the terms of the Creative Commons CC BY-NC-ND license (color online).

thermodynamic variable. Examining Reaction [1] shows that increasing [pct M] increases the $T_{M_xO_y}^{Fe}$. The equilibrium constant of Reaction [1] is:

$$K_{(1)} = \exp\left(-\frac{\Delta G_{(1)}^{\circ}}{RT}\right) = \exp\left(-\frac{\Delta H_{(1)}^{\circ} - T \times \Delta S_{(1)}^{\circ}}{RT}\right)$$

[3]

$$= \frac{P_{CO}^y a_{\underline{M}}^x}{a_{M_xO_y}(a_{\underline{C}})^y} = \frac{P_{CO}^y (f_M \times [\text{pct M}])^x}{a_{M_xO_y}(a_{\underline{C}})^y}$$

[4]

Therefore,

$$-\frac{\Delta H_{(1)}^{\circ}}{RT} + \frac{\Delta S_{(1)}^{\circ}}{R} = y \log P_{CO} + x \log f_M + x \log[\text{pctM}] - \log a_{M_xO_y} - y \log a_C$$

[5]

If the P_{CO}, $a_{M_xO_y}$, and a_C are reasonably assumed to be constants, respectively, and the $\Delta H_{(1)}^{\circ}$, $\Delta S_{(1)}^{\circ}$, and the activity coefficient f_M are assumed not to be changed significantly by T, then Eq. [5] is further simplified to:

$$-\frac{\Delta H_{(1)}^{\circ}}{RT} + \frac{\Delta S_{(1)}^{\circ}}{R} \approx x \log[\text{pctM}] + \text{constant},$$

[6]

which shows that $\log[\text{pct M}]$ is proportional to $1/T$. Here, the T corresponds to $T_{M_xO_y}^{Fe}$ where the oxide M_xOy starts to decompose by the carbothermic reaction. Therefore, it can be seen that increasing [pct M] increases $T_{M_xO_y}^{Fe}$. Moreover, O content (which must be [S.O]) is not a controlling thermodynamic variable for the carbothermic reaction.

Krasovskii and Griorovich reported a series of thermodynamic analyses for *non-isothermal* reduction of oxide inclusions in C-saturated liquid metal (Fe or Ni).[22] Although they considered an additional possibility of formation of metal carbides, it was not considered in the present study, because it would happen at considerably high content of the metal in the liquid steel.

III. THERMODYNAMIC ANALYSIS OF CARBOTHERMIC REACTIONS OF VARIOUS OXIDE INCLUSIONS IN LIQUID STEEL

In the present study, FactSage thermodynamic software with FSStel, FTOxid, and FactPS databases were used to analyze the carbothermic reactions for each oxide inclusion in liquid steel.[23,24] Therefore, the simplification made in Eq. [6] is not necessary, and more quantitative calculations could be carried out.

A. *Al₂O₃ Inclusion*

Figure 2 shows calculated phase diagrams for Al_2O_3 reduction in a C-saturated liquid steel. For illustration purposes, [pct Al] was set to 0.04. To meet the condition inside the gas fusion chamber where $P^{\dagger}$ is in the range of

---

†$P = P_{CO} + P_{CO_2} + \cdots = 1$ where $P_{CO} \approx 1$.

---

1 to 2 atm, P was set to 1 atm (Figure 2(a)) and 2 atm (Figure 2(b)), respectively. The thick line in each figure represents the zero-phase fraction (ZPF) line of Al_2O_3.[25,26] Upon heating, the Al_2O_3 starts to decompose by the carbothermic reaction on the line. The horizontal line $a - a'$ represents a temperature where the
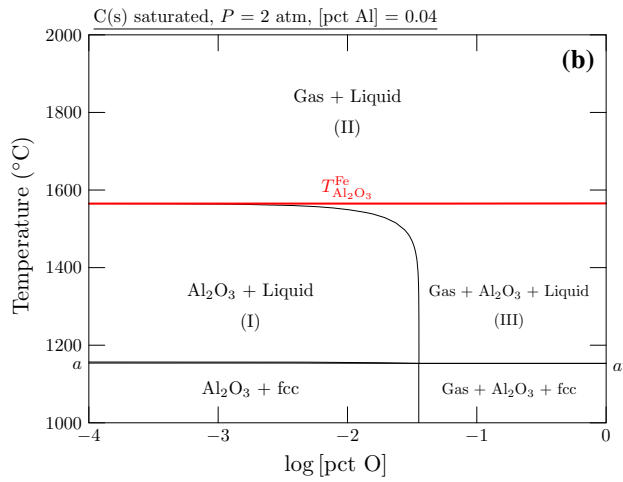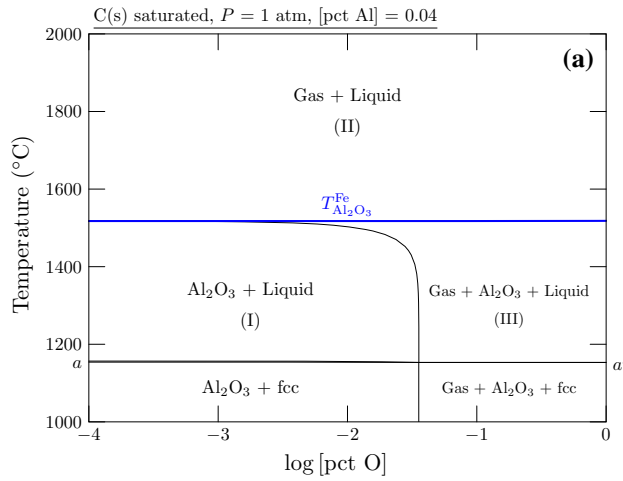
Fig. 2—Calculated phase diagrams of Fe-Al-C-O system under C saturation, [pct Al] = 0.04, (a) P = 1 atm and (b) P = 2 atm (color online).

steel specimen melts under the C saturation condition. In regions (I) and (III), the Al_2O_3 is still stable and is not reduced by C. Only O in the liquid steel (after melting in the graphite crucible) reacts with C according to Reaction [2]. In region (I), the "gas" phase is not seen as a stable phase, because its pressure is lower than the total pressure (either 1 atm or 2 atm). In reality, the CO(g) by Reaction [2] is generated at lower pressure and is carried out to the NDIR sensor by the carrier He gas. In this condition, O in the liquid steel is almost extracted because of the C saturation condition. This eventually provides the [S.O]. In region (II), the Al_2O_3 is reduced, and P_{CO} is higher than the total pressure P. If the O has already been extracted at a lower temperature, the additional CO(g) evolved in region (III) will correspond to the [I.O]. The temperature at the horizontal ZPF line is $T_{Al_2O_3}^{Fe}$. Therefore, by setting T_L below $T_{Al_2O_3}^{Fe}$ and T_H above $T_{Al_2O_3}^{Fe}$, the [S.O] and [I.O] can be separately measured in a single run of the two-stage gas fusion analysis. The calculated equilibrium mass of Al_2O_3 and P_{CO} at each temperature are shown in Figure 3 for the case of P = 2 atm. It is seen that Al_2O_3 does not decompose below $T_{Al_2O_3}^{Fe}$, but decomposes completely above $T_{Al_2O_3}^{Fe}$.
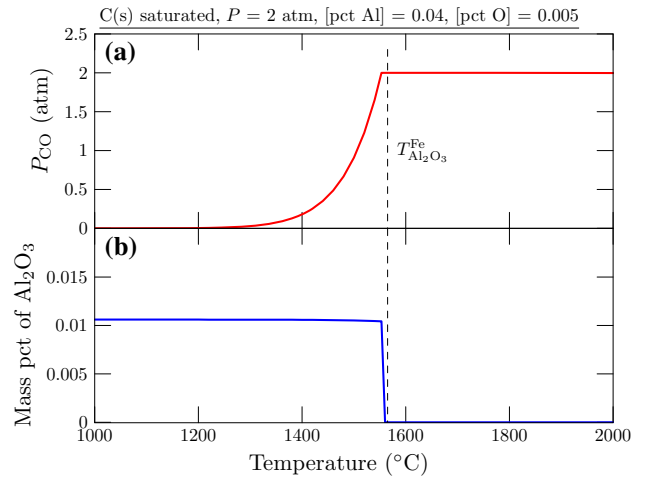

Fig. 3—Change of (a) partial pressure of CO(g) and (b) mass pct of Al_2O_3 in the steel at P = 2 atm of the steel specimen containing 0.04 pct Al and 0.005 pct O (color online).
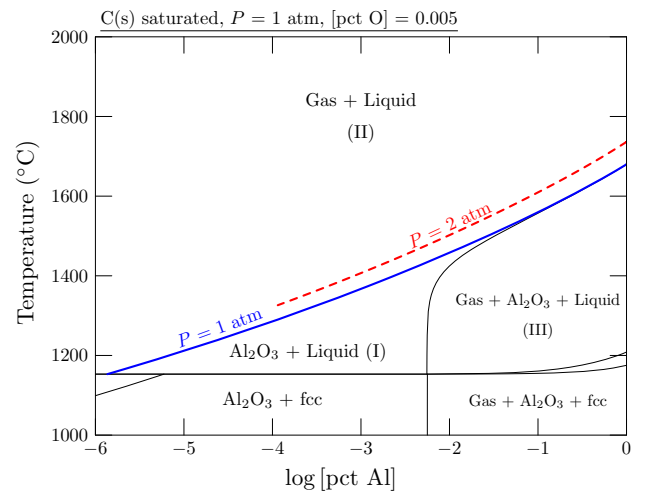

Fig. 4—A calculated phase diagram of Fe-Al-C-O system under C saturation, P = 1 atm, [pct O] = 0.005. The blue thick line represents the $T_{Al_2O_3}^{Fe}$ at 1 atm, and the red dashed thick line represents that of P = 2 atm (color online).

In regions (III) in Figure 2, P_{CO} is already higher than the total pressure due to high O content in the steel specimen. Even in this region, the extracted O to the gas phase is almost soluble O.

The $T_{Al_2O_3}^{Fe}$ at P = 2 atm was higher than that at P = 1 atm by approximately 45–50 K (45–50 °C). Accurate determination of the P depends on the setting of each gas fusion analysis chamber. In the present study (LECO ON-836), it was approximately 1.5 atm.[7]

Figure 2 shows that $T_{Al_2O_3}^{Fe}$ was almost independent of [pct O] at a given [pct Al], as was already discussed in Section II. Figure 4 shows a phase diagram of the same system at P = 1 atm where [pct Al] was used as the thermodynamic composition variable for the abscissa, while [pct O] was set to 0.005. At P = 2 atm, a similar trend can be found (a dashed line). Therefore, it is clear that the $T_{Al_2O_3}^{Fe}$ should be considered as a function of [pct
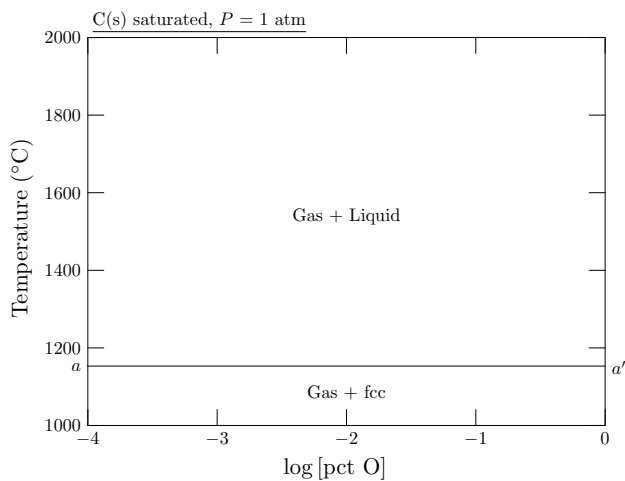
Fig. 5—A calculated phase diagram of Fe-C-O system under C saturation, $P = 1$ atm. Fe$_t$O cannot be stable under this condition.

Fig. 6—Calculated phase diagram of Fe-Si-C-O system under C saturation, $P = 1$ atm [pct Si] = 0.2. The blue thick line represents the $T_{SiO_2}^{Fe}$ at 1 atm, and the red dashed thick line represents that of $P = 2$ atm (color online).

Al]. This is in agreement with the report by Krasovskii and Griorovich.[22] For typical ULC steel grade where Al content is about 0.03 to 0.04 pct, the $T_{Al_2O_3}^{Fe}$ is roughly estimated to be in the range of 1773 K (1500 °C) to 1873 K (1600 °C). Therefore, the two isothermal temperature T_L and T_H should be selected by considering this temperature. It is reasonable that the T_L for Al$_2$O$_3$ should not be too much lower than $T_{Al_2O_3}^{Fe}$, in order to have rapid completion of Reaction [2]. In addition, it is better to set T_H as high as possible to reduce the Al$_2$O$_3$ completely.[27–29]

B. Fe$_t$O Inclusion

Figure 5 shows a calculated phase diagram for Fe$_t$O reduction in a C-saturated liquid steel. The Fe$_t$O may be found to be an inclusion in highly oxidized steel or may be regarded as surface scale.[30] As seen in the figure, the Fe$_t$O could not be stable under the C saturation condition. It was reduced even before the steel specimen melted. Therefore, two-step gas fusion analysis cannot be used to extract [S.O] in the case of steels containing Fe$_t$O inclusion. It may be used to measure the surface scale-type O content as Ise et al. proposed,[30] where they applied a non-isothermal heating method in the gas fusion analysis method.

C. SiO$_2$ Inclusion

Figure 6 shows a calculated phase diagram for SiO$_2$ reduction in a C-saturated liquid steel containing 0.2 pct Si. Similarly to the case of Al$_2$O$_3$ inclusion shown in Figure 2, regions (I), (II), and (III) were identified. $T_{SiO_2}^{Fe}$ was found to be in the range of 1509 K (1236 °C) to 1558 K (1285 °C), which is slightly above the melting temperature of the steel specimen ($a - a'$). Therefore, it is concluded that [S.O] and [I.O] in Si-killed steel where SiO$_2$ is the major inclusion can be measured separately from the thermodynamic view point. However,
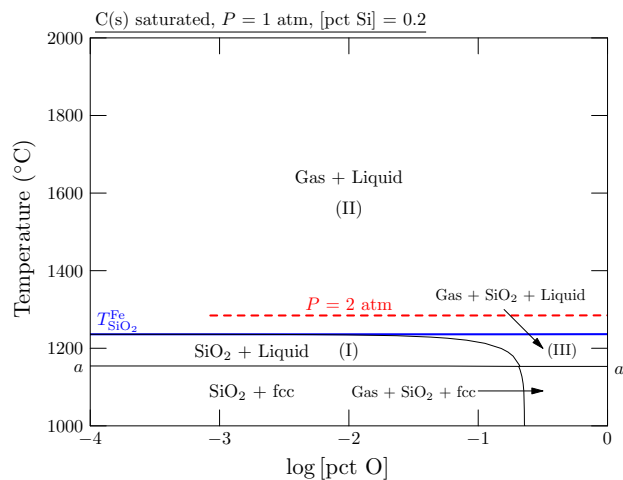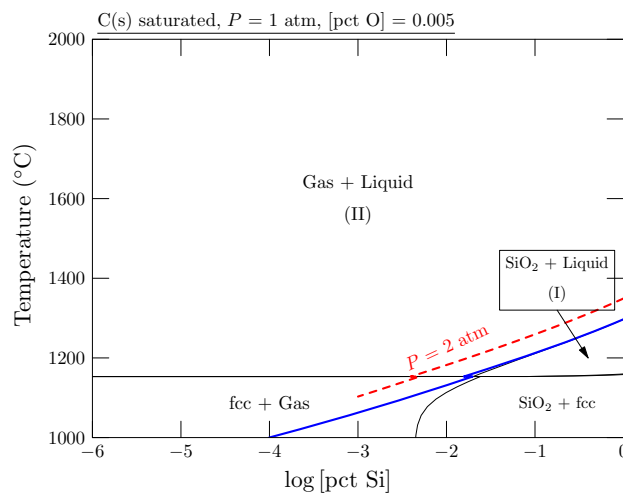

Fig. 7—Calculated phase diagram of Fe-Si-C-O system under C saturation, $P = 1$ atm [pct O] = 0.005. The blue thick line represents the $T_{SiO_2}^{Fe}$ at 1 atm, and the red dashed thick line represents that of $P = 2$ atm (color online).

separation of the [S.O] may take a longer time because of the lower T_L. Figure 7 shows the $T_{SiO_2}^{Fe}$ as a function of [pct Si].

D. CaO or MgO Inclusions

Similar thermodynamic analyses were carried out for CaO and MgO as oxide inclusions in Ca- or Mg-deoxidized steel which are known to be very complicated [31–35]. Figures 8(a) and (b) shows the calculated phase diagrams for CaO and MgO reduction in C-saturated liquid steels. Similarly to the case of Al$_2$O$_3$ and SiO$_2$ inclusions, regions (I) and (II) were identified. If Ca or Mg contents in liquid steel were thought to be in the range of 0.001 to 0.01 pct, T_{CaO}^{Fe} and T_{MgO}^{Fe} were roughly
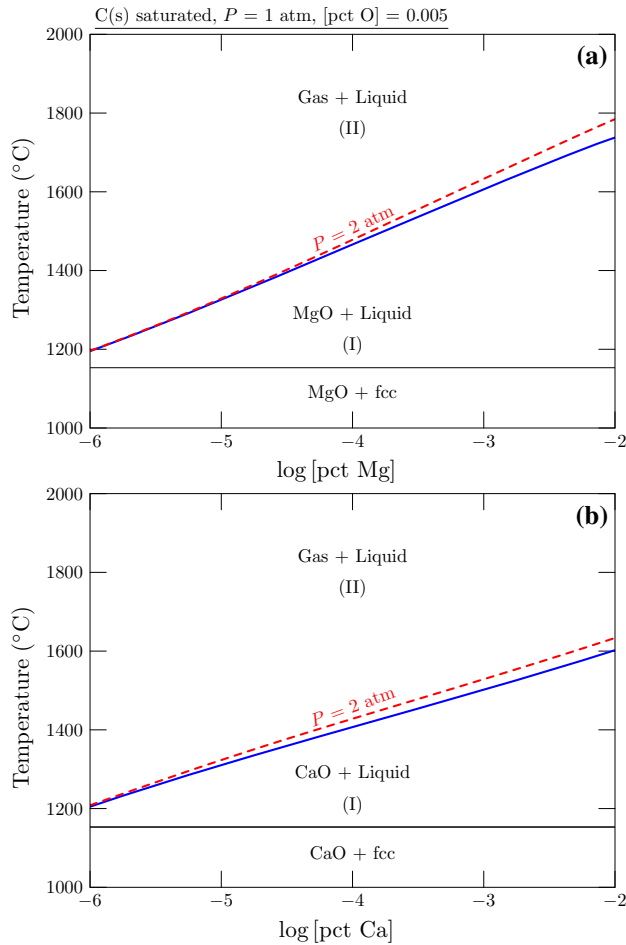
Fig. 8—Calculated phase diagrams of (*a*) Fe-Ca-C-O system and (*b*) Fe-Mg-C-O system under C saturation, P = 1 atm, [pct O] = 0.005. The blue thick line represents the T_{MgO}^{Fe} and T_{CaO}^{Fe} at 1 atm, and the red dashed thick line represents that of P = 2 atm (color online).

estimated to be 1873 K (1600 °C) to 1973 K (1700 °C) and 1773 K (1500 °C) to 1873 K (1600 °C), respectively. According to the present thermodynamic analyses, separate measurement of [S.O] and [I.O] may be possible.

IV. DISCUSSION

A. Stability of Al_2O_3 Inclusion Near $T_{Al_2O_3}^{Fe}$

Contrary to the conventional one-stage gas fusion analysis, the two-stage gas fusion analysis assumes that oxide inclusion is stable and is not reduced below $T_{M_xO_y}^{Fe}$. Although this fact is predicted by the thermodynamic analysis in the previous section, a dissolution experiment of oxide inclusion in C-saturated liquid steel was carried out for validation. Al_2O_3 inclusion was chosen as a representative oxide inclusion in liquid steel. A small alumina particle was put on an electrolytic Fe specimen, which was preliminarily saturated

by C. The specimen was charged in a graphite crucible (ID 9 mm) and was installed in a gold image furnace equipped with confocal scanning laser microscopy (CSLM, VL-2000DX-SVF17SP, Yonekura Manufacturing Co., Ltd., Japan). Ar gas (99.999 pct. purity) was cleaned by passing Drierite and Mg chip heated at 773 K (500 °C) to remove moisture and trace O in the Ar gas and then flowed into the chamber. A vacuum pump was used to evacuate the chamber, and the chamber was back-filled by the cleaned Ar gas. The evacuated chamber was kept for 20 s, and the pressure inside the chamber was read by an installed gauge. This ensured that there was no leak. This step was repeated three times. Then, the Ar gas flowed during the observation. The sample in the graphite crucible was heated by a halogen lamp inside the chamber as usual. The specimen was heated to 1873 K (1600 °C), and the floated Al_2O_3 particle was observed. The image was recorded and was post-processed to determine the size change of the Al_2O_3 particle, if any. An equivalent radius R_{eqv} was extracted using Image J software.[36,37] The observation was continued up to 450 s, which is three times longer than the time used for isothermal heating at T_L for Al_2O_3 inclusion in the previous study of the present authors.[8] The results are shown in Figure 9. The size of the Al_2O_3 inclusion did not change noticeably during the 450 s, even at slightly higher temperature than $T_{Al_2O_3}^{Fe}$. This observation indicates that there was a kinetic constraint on the carbothermic reduction: insufficient thermal driving force. The slow kinetics was also previously recognized. Khanna *et al.* reported that Fe droplets on Al_2O_3–C substrate started to react with each other after 1800 s at 1823 K (1550 °C).[38] The 1800 seconds is a considerably longer time than the time interval considered in the present study. Therefore, it can be safely assumed that at T_L, which is below $T_{Al_2O_3}^{Fe}$, the Al_2O_3 inclusion is stable, and only [S.O] can be separately measured. For other oxide inclusions considered in the present article, similar validation may be carried out.

B. Calculation of [S.O] and [I.O] from NDIR Intensity Data

A ULC steel sample was prepared in the present study by melting electrolytic iron and Al shot in an alumina crucible at 1873 K (1600 °C) under deoxidized Ar gas in an induction furnace. Total Al content was approximately 0.04 pct. The liquid steel was sampled by a quartz tube and was treated for the gas fusion analysis. The analysis for O content was carried out by LECO ON-836 (St Joseph, MI). The detailed procedure can be found elsewhere.[8] Since the electrolytic iron inherently contains a certain content of O (< 150 ppm), the prepared steel specimen contained both soluble and insoluble O. Figure 10 shows the intensity of O in the ULC steel specimen, which was post-corrected for background and blank data. The area below the curve is "adjusted area" (A_{adj}) and is correlated to the mass of the analyte (G) as[7,39]:
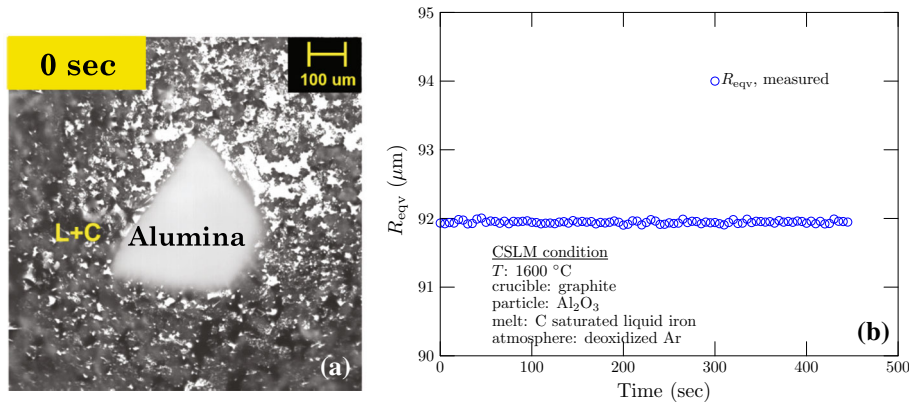
Fig. 9—The result of CSLM observation for the dissolution of Al_2O_3 in C-saturated liquid steel at 1873 K (1600 °C): (a) a still image and (b) change of the particle size, R_{eqv} (color online).
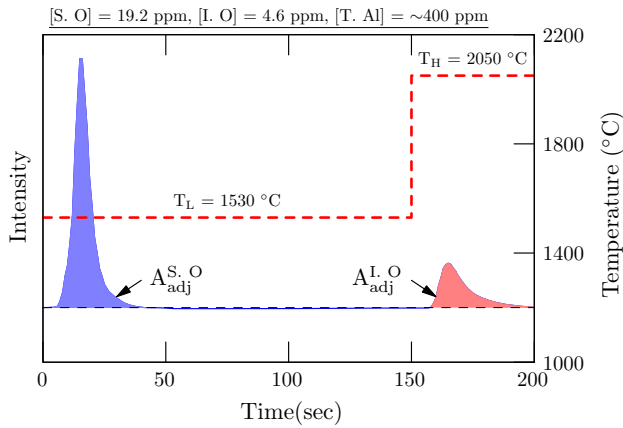

Fig. 10—A background corrected intensity of O (in the form of CO) from the ULC steel specimen was obtained by the two-stage gas fusion analysis. $A_{adj}^{S.O}$ and $A_{adj}^{I.O}$ are marked (color online).

$$A_{adj} = k_1 \times G + k_2 \qquad [7]$$

The present authors proposed to separate the above calculation into two stages[8]:

$$A_{adj}^{S.O} = k_1 \times G^{S.O} + k_2 \qquad [8]$$

$$A_{adj}^{I.O} = k_1 \times G^{I.O} + k_2 \qquad [9]$$

From the mass of each analyte (soluble and insoluble O in the present case), content of each O ([S.O] and [I.O]) could be obtained. The mass of the specimen used in this trial was 0.6023 g, and the obtained [S.O] and [I.O] were 19.2 ppm and 4.6 ppm, respectively. The proposed two-stage gas fusion analysis was already tested and validated for various ULC steel specimens.[8] Typical range of analytical uncertainty was also reported,[8] which was in a reasonable range

of oxygen analyses in steel specimens. The uncertainty was due to not only the analytical procedure but also the specimen itself. The latter may be attributed to irregular presence of non-metallic inclusions in the specimen. For other steel grades (low, mid, and high C steels), new results will be shown subsequently in a separate article.[18]

A slightly different approach was also reported. Grigorovitch *et al.* proposed the fractional gas analysis method in which a steel specimen is heated in a "non-isothermal" way to extract O from different types of oxide inclusions.[40,41] In this approach, the deconvolution of the intensity peaks was applied as was done in the present study.

C. Possible Range of $T_{M_xO_y}^{Fe}$ for the Various Oxide Inclusions

Given that the chamber pressure would be in a range of 1 to 2 atm, which depends on the condition of the gas fusion analyzer, the possible range of $T_{M_xO_y}^{Fe}$ was summarized for each oxide considered in the present study (M_xO_y = Al_2O_3, SiO_2, MgO, and CaO), as shown in Figure 11. Metal content ([pct M], M = Al, Si, Mg, and Ca) was chosen to be in a range of practical interest. For each filled box, the upper and lower limits of the temperature represent $T_{M_xO_y}^{Fe}$ at 2 atm and 1 atm, respectively. Therefore, after identifying the possible range of $T_{M_xO_y}^{Fe}$, T_L and T_H should be selected as follows. T_L should be chosen to be close to the range (as high as possible to accelerate Reaction [2]). T_H can be set to a higher temperature than $T_{M_xO_y}^{Fe}$ (as high as possible to complete Reaction [1]). For Al_2O_3 inclusion in a ULC steel ([pct Al] ≈ 0.03 to 0.04), the present authors chose 1530 °C for the T_L, which is shown in the figure by a closed circle. It was shown that the proposed two-stage gas fusion analysis was reliable and promising to simultaneously measure soluble and insoluble O in steel specimens.[8,18]
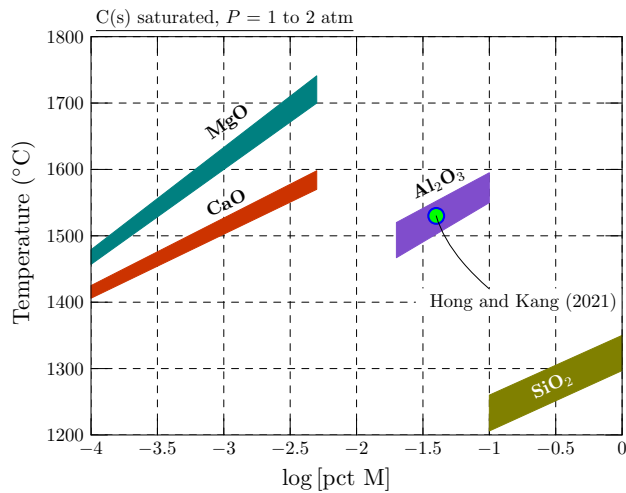
Fig. 11—Estimated regions of $T_{M_xO_y}^{Fe}$ for the various oxide inclusions considered in the present study (Al_2O_3, SiO_2, MgO, and CaO). Each colored region represents the possible range of $T_{M_xO_y}^{Fe}$, which may be considered as a function of [pct M] (chosen in a practically meaningful range) and P (1 to 2 atm) (color online).

V. CONCLUSIONS

A series of thermodynamic analyses were carried out to determine optimum conditions for the two-stage gas fusion analysis, which allows the simultaneous analysis of soluble and insoluble O contents in steel specimens. The present thermodynamic analysis provides theoretical evidence of the recently proposed "two-stage" gas fusion analysis method.[8] Commercial CALPHAD software and databases were used to find the conditions for the following oxide inclusions: Al_2O_3, SiO_2, Fe_tO, CaO, and MgO. The following points were found:

1. A specific temperature ($T_{M_xO_y}^{Fe}$) could be found. Below this temperature, the oxide inclusion is not reduced by C. Therefore, only soluble O in the steel matrix could be extracted as CO(g), which is then detected by the NDIR sensor to count [S.O] in the steel specimen.
2. Above this temperature, the oxide inclusion could be successfully reduced by the carbothermic reaction. The subsequently generated CO(g) provides the basis of [I.O] in the steel specimen.
3. The specific temperature for each inclusion did not depend on the O content, but did depend on the content of the deoxidizing element M ([pct M]): the temperature increased with the increase of [pct M]. Moreover, the pressure inside the carbothermic reaction chamber also increased the specific temperature.
4. The method could be successfully applied in Al-killed steel in which Al_2O_3 is the main inclusion.
5. Among other pure oxides considered, Fe_tO was reduced easily by C, even before the steel specimen melts. In this case, the method could not be applied.

In the case of the alumina, an experiment was carried out to confirm its stability under the carbothermic reducing environment. Alumina was not reduced even at a slightly higher temperature than the specific temperature. This lends strong support to the method proposed[8] in which soluble O in the steel matrix could be separately extracted to obtain [S.O] in the steel specimen.

CONFLICT OF INTEREST

The authors declare that they have no conflict of interest.

REFERENCES

1. Q. Ren, Y. Zhang, L. Zhang, J. Wang, Y. Chu, Y. Wang and Y. Ren: *J. Mater. Res. Tech.*, 2020, vol. 9, pp. 5648–65.
2. L. Zhang and B. Thomas: *Metall. Mater. Trans. B*, 2006, vol. 37B, pp. 733–61.
3. Y. Sahai: *Metall. Mater. Trans. B*, 2016, vol. 47B, pp. 2095–2106.
4. B.A. Webler and P.C. Pistorius: *Metall. Mater. Trans. B*, 2020, vol. 51B, pp. 2437–52.
5. J.H. Park and L. Zhang: *Metall. Mater. Trans. B*, 2020, vol. 51B, pp. 2453–82.
6. S. Imashuku and K. Wagatsuma: *Metall. Mater. Trans. B*, 2020, vol. 51B, pp. 79–84.
7. ON836 Oxygen/Nitrogen Analyzer Instruction Manual, version 1.9.x Edition, LECO Corp., 3000 Lakeview Ave., St. Joseph, MI 49085 2013.
8. H.-M. Hong and Y.-B. Kang: *ISIJ Int*., 2021, vol. 61, pp. 2464–73.
9. Y.-M. Cho, W.-Y. Cha and Y.-B. Kang: *Metall. Mater. Trans. B*, 32021, vol. 52, pp. 3032–44.
10. H. Hoff and H. Lessing: *Stahl u. Eisen*, 1956, vol. 76, pp. 1442–52.
11. Y. Yoshida and Y. Funahashi: *Tetsu-to-Hagane*, 1975, vol. 61, pp. 2489–500.
12. K. Morinaga, A. Oba and Y. Itoh: *Tetsu-to-Hagane*, 1963, vol. 49, pp. 1663–68.
13. M. Kuba, K. Tasaka, Y. Itoh and H. Maede: *Tetsu-to-Hagane*, 1972, vol. 58, pp. 1504–10.
14. Y. Yoshida and Y. Funahashi: *Trans. ISIJ*, 1976, vol. 16, pp. 628–36.
15. E.T. Turkdogan and R.J. Fruehan: *Steel Res.*, 1972, vol. 11, pp. 371–84.
16. G. Li and H. Suito: *Metall. Mater. Trans. B*, 1997, vol. 28B, pp. 251–58.
17. E.T. Turkdogan, *Steel Res.*, 1991, vol. 62, pp. 379–82.
18. Y.-M. Cho, D.-J. Lee, H.-J. Cho, W.-Y. Kim, S.-W. Han and Y.-B. Kang: *ISIJ Int.*, 2022, vol. 62. No. 6, in press.
19. O. Adaba, R.J. O'Malley and L.N. Bartlett: *Metall. Mater. Trans. B*, 2022, vol. 51B, pp. 1406–17.
20. H. Suito: *Proc. E. T. Turkdogan Symp.*, 1994, pp. 141–52.
21. H. Suito, H. Inoue and R. Inoue: *ISIJ Int.*, 1991, vol. 31, pp. 1381–88.
22. P.V. Krasovskii and K.V. Grigorovich: *Russ. Metall.*, 2002, vol. 2002, pp. 108–113. .
23. C.W. Bale, E. Bélisle, P. Chartrand, S.A. Decterov, G. Eriksson, K. Hack, I.-H. Jung, Y.-B. Kang, J. Melançon, A.D. Pelton, C. Robelin and S. Petersen: *Calphad*, 2009, vol. 33, pp. 295–311.
24. C.W. Bale, E. Bélisle, P. Chartrand, S.A. Decterov, G. Eriksson, A.E. Gheribi, K. Hack, I.H. Jung, Y.B. Kang, J. Melançon, A.D. Pelton, S. Petersen, C. Robelin, J. Sangster, P. Spencer and M.-A. Van Ende: *Calphad*, vol. 54, pp. 35–53.
25. H. Gupta, J.E. Morral and H. Nowotny: *Scripta Metall.*, 1996, vol. 20, pp. 889–94. .
26. A.D. Pelton, Ch. 7: General phase diagram sections, in *Phase Diagrams and Thermodynamic Modeling of Solutions*. ed. by A.D. Pelton (Elsevier, Amsterdam, 2019), pp. 103–131.
27. F.R. Bryan and S. Bonfiglio: *J. Chromatographic Sci.*, 1964, vol. 2, pp. 97–101.
28. F.M. Evens: A New Technique for the Determination of Oxygen and Nitrogen in Steel, Ph.D. thesis, Iowa State University, Ames, 1962.

29. J.G. Thompson and V.C. Holm: Determinations of Oxygen in Alloy Steels, Tech. Rep. Research Paper PR1115, National Bureau of Standards, 1938.
30. T. Ise, Y. Nuri, Y. Kato, T. Ohishi and H. Matsunaga: *ISIJ Int.*, vol. 38, pp. 1362–68.
31. T. Kimura and H. Suito: *Metall. Mater. Trans. B*, 1994, vol. 25, pp. 33–42.
32. J.-D. Seo and S.-H. Kim: *Steel Res.*, 2000, vol. 71, pp. 101–06.
33. S. Gustafsson and P.-O. Mellberg, *Scand. J. Metall.*, 1980, vol. 9, pp. 111–16.
34. I.-H. Jung, S. Decterov and A.D. Pelton: *Metall. Mater. Trans. B*, 2004, vol. 35, pp. 493–507.
35. Y.-B. Kang: *Metall. Mater. Trans. B*, 2019, vol. 50, pp. 2942–58.
36. ImageJ, Version 1.45s, developed at U.S. National Institutes of Health. Available at: http://imagej.nih.gov/ij/.
37. D.-H. Kim, J.-B. Choi, H.-M. Hong, Y.-M. Cho, Y.-J. Park, M.-H. Song and Y.-B. Kang: *Met. Mater. Int.*, 2022, in press, https://doi.org/10.1007/s12540-022-01190-z.
38. R. Khanna, M. Ikram-Ul Haq, Y. Wang, S. Seetharaman and V. Sahajwalla: *Metall. Mater. Trans. B*, 2011, vol. 42, pp. 677–84.
39. P.V. Krasovskii, W. Gruner and K.V. Grigorovitch: *Steel Res.*, 2006, vol. 77, pp. 64–72 .
40. K.V. Grigorovitch, O. Komolova and D. Gorkusha: *Proc. 5th Int. Conf. on Process Development in Iron and Steelmaking (SCAN-MET-V)*, 2016, Swerea/MEFOS, Luleå.
41. D. Gorkusha, A.V. Karasev, O. Komolova, K.V. Grigorovitch and P. Jönsson, *ISIJ Int.*, 2020, vol. 60, pp. 2819–28.